Journal of Solid State Chemistry 182 (2009) 509–516

Contents lists available at ScienceDirect

Journal of Solid State Chemistry

journal homepage: www.elsevier.com/locate/jssc

Synthesis and crystal structure determination of yttrium ultraphosphate YP_5O_{14}

A. Mbarek [a,b], M. Graia [c,*], G. Chadeyron [b], D. Zambon [b], J. Bouaziz [a], M. Fourati [a]

[a] Laboratoire de Chimie Industrielle, Ecole Nationale d'Ingénieurs de Sfax, Université de Sfax, BP W 3038, Sfax, Tunisie
[b] Laboratoire des Matériaux Inorganiques (UMR CNRS 6002), Université Blaise Pascal et ENSCCF, F-63177 Aubière Cedex, France
[c] Laboratoire de Matériaux et de Cristallochimie, Faculté des Sciences de Tunis, Université de Tunis-El Manar, 2092 El Manar II Tunis, Tunisie

ARTICLE INFO

Article history:
Received 13 April 2008
Received in revised form
8 November 2008
Accepted 15 November 2008
Available online 3 December 2008

Keywords:
Ultraphosphate
Rare-earth ions
Crystal structure
Optical properties

ABSTRACT

The crystal structure of monoclinic YP_5O_{14} (space group $C2/c$, $a = 12.919(2)$ Å, $b = 12.796(4)$ Å, $c = 12.457(2)$ Å, $\beta = 91.30(1)^\circ$, $Z = 8$) has been refined from single-crystal X-ray diffraction data. Full-matrix least-squares refinement on F^2 using 2249 independent reflections for 183 refinable parameters results in a final R value of 0.027 ($\omega R = 0.069$). The structure is isotypic with HoP_5O_{14}. This structure is built up from infinite layers of PO_4 tetrahedra linked through isolated YO_8 polyhedra. The three-dimensional cohesion of the framework results from Y–O–P bridges. This crystal structure refinement leads to the calculated X-ray diffraction powder pattern of this monoclinic polymorph, which has been the starting point of a thorough study of the solid-state synthesis of this ultraphosphate. This investigation further leads to a better outstanding of features observed during the synthesis of powdered samples. The thermal behavior of this ultraphosphate has been studied by DTA and TGA analyses. The infrared and Raman spectroscopic characterizations have been carried out on polycrystalline samples. The luminescence properties of the Eu^{3+} ion incorporated in the monoclinic $C2/c$ polymorph of YP_5O_{14} as local structural probe show that in YP_5O_{14}: 5% Eu^{3+} sample, the Eu^{3+} ions are distributed over the two Y^{3+} crystallographic sites of C_2 symmetry of this structure.

1. Introduction

Ultraphosphates of LnP_5O_{14} formula (Ln = rare-earth elements) have been proved to be attractive matrices for lasing materials [1,2] or rare-earths sensitizer-activator pairs containing phosphors for the energy upconversion [3]. For some of these applications it can be preferable to use matrices with low active rare-earth content. For this purpose, La and Y may be used to dilute the active rare earths. For instance, for the energy upconversion involving transfers between Yb^{3+} and Er^{3+} ions, the yttrium, the crystal-chemical properties of which are closely related to those of the heavier rare earths, can be better appropriated. Although the existence of the YP_5O_{14} ultraphosphate has been mentioned for a long time [4–6], no thorough crystallographic study has been carried out till date. These pioneering works mentioned a polymorphism for this compound but some inconsistencies have been pointed out in the literature. For example, Fedorova et al. [7] did not mention any polymorphic transition and reported this compound as being stable up to 1400 °C whereas Agrawal and Hummel [8] claimed that this compound only exhibits a monoclinic form with an incongruent melting at 860±10 °C yielding $Y(PO_3)_3$ and P_2O_5.

Due to the primordial role played by the host matrices when optical properties are taken up, it becomes essential to clearly identify the polymorphs and their conditions of appearance. In the present case the ideal thing would be to bring under control the solid-state synthesis of the title compound. To that end a new investigation of this compound has been undertaken in order to clarify the afore-mentioned discrepancies and to optimize the polymorphs preparation. During the synthesis of this compound colorless single crystals of the $C2/c$ monoclinic form have been obtained and this paper deals with the crystal structure refinement of this polymorph. The thermal behavior of this ultraphosphate has also been investigated by coupled TGA–DTA scans, thermal treatments and X-ray diffraction. Some preliminary luminescence properties of the Eu^{3+} ion incorporated as local structural probe have been investigated at room temperature. IR and Raman spectroscopic characterizations have been carried out.

2. Experimental

2.1. Syntheses

Single crystals of YP_5O_{14} have been obtained using phosphoric acid as an etchant for Y_2O_3. A mixture of H_3PO_4 (containing 15% of water by weight, Riedel De Haen) and Y_2O_3 (Rhône-Poulenc,

* Corresponding author. Fax: +216 71 88 50 08.
E-mail address: mohseng2002@yahoo.fr (M. Graia).

0022-4596/$ - see front matter © 2008 Elsevier Inc. All rights reserved.
doi:10.1016/j.jssc.2008.11.021

99.99%) in a molar ratio of 45:1, was set in an alumina crucible and heated in air in a muffle furnace. The crucible was heated up to 600 °C, held at this temperature for 5 h, then the temperature was raised up to 650 °C for additional 17 h, before shutting the furnace power off. After cooling and washing, the sample with a large amount of hot water, lots of prismatic crystals of YP_5O_{14} were recovered.

For physical–chemical and optical characterizations, samples of YP_5O_{14} have been synthesised in the solid state by reacting yttrium oxide with ammonium dihydrogen phosphate (Touzart and Matignon, 99%) in a graphite crucible. Molecular excesses of $(NH_4)H_2PO_4$ from 15% to 40% were used for these syntheses. The mixtures were first heated at 300 °C for 12 h. Then the temperature was raised at values between 450 and 650 °C, depending on the batches and the mixtures were held at these temperatures for additional 48 h before finally cooling to room temperature.

In all the syntheses the YP_5O_{14} ultraphosphate is only obtained as crystals with needle or/and platelet-like shapes and extracted from the batch by washing with hot water. No powdered part of the sample can be obtained. Therefore polycrystalline samples are obtained by crushing the crystals. Let us mention that crystals are stable towards water, ethanol and isoamyl acetate, so that they can abundantly be washed before crushing or grinding.

For optical measurements, Eu^{3+}-doped samples $Y_{1-x}Eu_xP_5O_{14}$ ($x = 0.05$) were obtained by substituting the Eu^{3+} ions for the Y^{3+} ones using appropriate amounts of europium oxide Eu_2O_3 (Rhône-Poulenc, 99.99%).

2.2. X-ray diffraction

X-ray diffraction powder patterns were recorded with a SIEMENS D501 diffractometer equipped with a back monochromator using the Cu$K\alpha$ radiation.

2.3. Thermal behavior

Thermal data for YP_5O_{14} were collected using a METTLER-TOLEDO TGA/SDTA analyzer. A sample of 45 mg was heated in air at 2 °C min^{-1} from room temperature to 1000 °C.

2.4. Infrared and Raman spectroscopies

Infrared spectra of powdered monoclinic $C2/c$ YP_5O_{14} polymorph were recorded with a Nicolet FTIR spectrometer equipped with an attenuated total reflection (ATR) accessory. MicroRaman diffusion spectra were recorded at room temperature using a Jobin Yvon T64000 spectrometer. The available excitation wavelength provided by an argon ion laser was 514.53 nm.

2.5. Optical measurements

The emission spectra were recorded at room temperature with a Jobin Yvon spectrofluorimeter, consisting of a TRIAX 180 in excitation and a TRIAX 550 in detection and equipped with a 400 W Xenon lamp and a CCD SYMPHONY detector.

3. Crystal data and structure determination

A suitable single crystal of YP_5O_{14} was selected and mounted on a thin glass fiber. Intensities measurement was carried out at room temperature using an Enraf Nonius CAD4 automated 4-circles diffractometer (Mo$K\alpha$ radiation, $\lambda = 0.71069$ Å). Data were corrected for Lorentz and polarization effects. An empirical absorption correction deduced from psi-scans has been applied. The structure was solved by the Patterson method using SHELXS86 [9] and subsequent difference Fourier syntheses and then refined by full-matrix least-squares method on F^2 using SHELXL97 [10].

Table 1
Crystallographic data, data collection, and refinement details for YP_5O_{14}.

Crystal data	
Formula weight (g)	467.76
Shape	Prismatic
Color	Colourless
Crystal dimensions (mm)	$0.25 \times 0.25 \times 0.50$
Crystal system	Monoclinic
Space group	$C2/c$
Cell parameters	
a (Å)	12.919(2)
b (Å)	12.796(4)
c (Å)	12.457(2)
β (deg.)	91.30(1)
V (Å^3)	2058.7(8)
Z	8
D_c (Mg m^{-3})	3.018
μ (Mo$K\alpha$) (mm^{-1})	6.53
Data collection	
Diffractometer	Enraf-Nonius CAD-4
Temperature(K)	293(2)
Scan mode	ω–2θ
θ range (deg.) for data collection	2.2–27.0
Limiting indices	$h = -16 \rightarrow 16$
	$k = -1 \rightarrow 16$
	$l = -15 \rightarrow 2$
Measured reflections	2999
Independent reflections	2249 [$R_{int} = 0.027$]
Refinement	Full-matrix least-squares on F^2
Refinement	
Parameters refined	183
Final R indices [$I > 2\sigma(I)$]	$R = 0.027$; $wR = 0.069$
Extinction coefficient	0.0045(2)
$s(F^2)$ Goodness-of-fit on F^2	1.11
$(\Delta\rho)_{max}$ and $(\Delta\rho)_{min}$ (e Å^{-3})	0.54 and −0.61
Weighting scheme: $w = 1/[\sigma^2(F_o^2)+(0.0258P)^2+8.7902P]$, where $P = (F_o^2+2F_c^2)/3$	

Details of the data collection, data reduction and structure refinement are listed in Table 1. Further details on the crystal structure may be obtained from the Fachinformationszentrum Karlsruhe, 76344 Eggenstein-Leopoldshafen, Germany, on quoting the depository number 419078.

4. Results and discussion

4.1. Crystal structure description

The atomic coordinates and anisotropic displacement parameters are given in Tables 2 and 3, respectively. Bond distances and angles are gathered in Table 4.

The YP_5O_{14} (monoclinic II, $C2/c$) structure is built up from infinite layers of PO_4 tetrahedra further linked through isolated YO_8 polyhedra. Accordingly the cohesion of the three-dimensional framework results from Y–O–P bridges.

These layers are parallel to the ab-plane and are stacked along the c-axis at distance of $c/2$. They are constituted of 8-membered corrugated rings of PO_4 tetrahedra involving P(2), P(3), P(4) and P(5) phosphorus atoms (Fig. 1). Each P_8O_{24} ring shares four $P(1)O_4$ bridging tetrahedra with each of four adjacent rings to form the infinite layer of PO_4 tetrahedra. Two kinds of PO_4 tetrahedra coexist in this structure. Two of them, belonging to the P_8O_{24} ring,

namely $P(2)O_4$ and $P(4)O_4$ are ternary tetrahedra sharing three of their oxygen atoms with three other PO_4 groups. They are regular enough with one short terminal P–O bond (1.462 and 1.464 Å, respectively) and three bridging ones ranging from 1.560 to 1.574 Å and from 1.557 to 1.574 Å, respectively. The other three PO_4 tetrahedra, $P(1)O_4$, $P(3)O_4$ and $P(5)O_4$ are called internal tetrahedra with only two oxygen atoms involved in P–O–P bonds. They are much more distorted than the preceding ones with two terminal (from 1.466 to 1.483 Å) and two bridging (from 1.616 to 1.640 Å) P–O bonds.

Both Y(1) and Y(2) crystallographically independent yttrium atoms are 8-coordinated by the oxygen atoms in archimedean antiprism and dodecahedral arrangements, respectively, with bond distances ranging from 2.322 to 2.363 Å and from 2.279 to 2.393 Å. The $Y(2)O_8$ dodecahedron is little bit more distorted than the $Y(1)O_8$ square antiprism. This may be closely related to the constraint induced by the three-dimensional connections since the $Y(2)O_8$ dodecahedra are linked by corner-sharing to five P_8O_{24} rings whereas the $Y(1)O_8$ ones are connected to three P_8O_{24} rings only.

Thereby the P_8O_{24} rings are linked to three $Y(1)O_8$ and five $Y(2)O_8$ polyhedra. More accurately each P_8O_{24} ring is firstly linked, on one side, by sharing corners involving O(12) and O(11), to an $Y(2)O_8$ dodecahedron through the two ternary $P(4)O_4$ and the two internal $P(3)O_4$ tetrahedra and, on the opposite side, to an $Y(1)O_8$ square antiprism by corner-sharing also through the two ternary $P(2)O_4$ tetrahedra attached in cis position on the O(9)–O(9) edge of this $Y(1)O_8$ polyhedron. Then the P_8O_{24} ring is further joined in the *ab*-plane by corner-sharing involving O(14) atoms to two other $Y(2)O_8$ dodecahedra through the two internal $P(5)O_4$ tetrahedra and to two other $Y(2)O_8$ groups lying on both sides of the *ab*-plane through the internal $P(3)O_4$ tetrahedra, by sharing O(11) corners.

It is now well known that the LnP_5O_{14} ultraphosphates are divided into four structural types labeled from I to IV in Fig. 2. In this figure are only mentioned results from single-crystal works and the main crystallographic characteristics of each of the four archetypes are displayed. In all these structural types the rare earths or yttrium trivalent cations are 8-coordinated by the oxygens and the shapes of their coordination polyhedra as presented in this figure have been specified according to the Porai-Koshits and Aslanov's criteria [26]. This point had already been discussed by Cole et al. [11] who reported that in monoclinic type I ($P2_1/c$) structures the polyhedron around the rare earth would be better described as a square antiprism rather than a bicapped trigonal prism as previously mentioned in NdP_5O_{14} [13]. In the orthorhombic type III (*Pnma*) structure these authors suggest this polyhedron as best described as a distorted bicapped trigonal prism, while in the triclinic IV (P1) structural type either of the two polyhedra could have been defined due to their highly irregular shapes. From our evaluations of the characteristic δ dihedral angles at the b type edges according to Porai-Koshits and Aslanov's criteria we agree with the Cole et al. description for these three structural types. With regards to the last one, i.e. monoclinic II ($C2/c$) type, our results diverge from those of Cole et al. who propose two square antiprisms surrounding the two independent trivalent ions whereas we found a dodecahedron and a square antiprism.

Table 2
Fractional atomic coordinates and equivalent isotropic displacement parameters (Å^2) for YP_5O_{14}.

Atom	*x*	*y*	*z*	U_{eq}
Y1	0	0.47883 (4)	0.25	0.0068 (1)
Y2	0	1.03131 (4)	0.25	0.0067 (1)
P1	0.14674 (7)	0.46604 (8)	−0.00122 (8)	0.0081 (2)
P2	0.14945 (7)	0.66787 (7)	0.10295 (8)	0.0073 (2)
P3	0.02500 (7)	0.84819 (8)	0.03270 (8)	0.0075 (2)
P4	−0.18183 (7)	0.86229 (7)	0.10887 (8)	0.0069 (2)
P5	0.32181 (7)	0.75046 (8)	0.24069 (8)	0.0080 (2)
O1	0.2506 (2)	0.3957 (2)	0.0084 (2)	0.0109 (5)
O2	0.1947 (2)	0.5815 (2)	0.0271 (2)	0.0102 (5)
O3	0.0865 (2)	0.7388 (2)	0.0217 (2)	0.0107 (6)
O4	0.2444 (2)	0.7369 (2)	0.1364 (2)	0.0119 (6)
O5	−0.0908 (2)	0.8015 (2)	0.0549 (2)	0.0106 (6)
O6	0.2407 (2)	0.7717 (2)	0.3356 (2)	0.0129 (6)
O7	0.1143 (2)	0.4629 (2)	–0.1147 (2)	0.0141 (6)
O8	0.0767 (2)	0.4346 (2)	0.0857 (2)	0.0141 (6)
O9	0.0894 (2)	0.6281 (2)	0.1923 (2)	0.0135 (6)
O10	0.0255 (2)	0.8975 (2)	−0.0738 (2)	0.0150 (6)
O11	0.0610 (2)	0.9030 (2)	0.1314 (2)	0.0121 (6)
O12	−0.1528 (2)	0.9504 (2)	0.1782 (2)	0.0130 (6)
O13	0.3840 (2)	0.8433 (2)	0.2175 (2)	0.0157 (6)
O14	0.3699 (2)	0.6497 (2)	0.2691 (2)	0.0155 (6)

$U_{éq} = (1/3)\Sigma_i\Sigma_j U_{ij} a^*_i a^*_j . a_i . a_j$.

Table 3
Anisotropic displacement parameters (Å^2) of YP_5O_{14}.

Atom	U_{11}	U_{22}	U_{33}	U_{12}	U_{13}	U_{23}
Y1	0.0065 (2)	0.0090 (3)	0.0050 (2)	0	−0.0000 (2)	0
Y2	0.0067 (2)	0.0083 (3)	0.0051 (2)	0	−0.0002 (2)	0
P1	0.0077 (4)	0.0100 (5)	0.0065 (5)	0.0020 (4)	−0.0004 (3)	0.0000 (4)
P2	0.0072 (4)	0.0089 (5)	0.0059 (5)	0.0005 (3)	−0.0002 (3)	0.0005 (4)
P3	0.0062 (4)	0.0097 (5)	0.0065 (5)	0.0013 (3)	0.0004 (3)	0.0009 (4)
P4	0.0053 (4)	0.0090 (4)	0.0064 (4)	0.0000 (3)	0.0000 (3)	0.0004 (4)
P5	0.0061 (4)	0.0102 (5)	0.0076 (5)	0.0000 (4)	0.000 (3)	−0.0023 (4)
O1	0.011 (1)	0.014 (1)	0.008 (1)	0.005 (1)	−0.002 (1)	−0.001 (1)
O2	0.010 (1)	0.009 (1)	0.012 (1)	0.000 (1)	0.003 (1)	−0.000 (1)
O3	0.011 (1)	0.012 (1)	0.010 (1)	0.004 (1)	−0.001 (1)	−0.001 (1)
O4	0.011 (1)	0.014 (1)	0.010 (1)	–0.003 (1)	−0.002 (1)	−0.001 (1)
O5	0.007 (1)	0.013 (1)	0.012 (1)	0.001 (1)	0.003 (1)	−0.000 (1)
O6	0.015 (1)	0.011 (1)	0.012 (1)	0.002 (1)	0.006 (1)	−0.001 (1)
O7	0.015 (1)	0.018 (1)	0.009 (1)	0.005 (1)	–0.005 (1)	−0.002 (1)
O8	0.015 (1)	0.016 (1)	0.011 (1)	–0.001 (1)	0.005 (1)	−0.001 (1)
O9	0.016 (1)	0.015 (1)	0.009 (1)	–0.004 (1)	0.004 (1)	−0.002 (1)
O10	0.018 (1)	0.016 (1)	0.011 (1)	0.003 (1)	0.001 (1)	0.004 (1)
O11	0.009 (1)	0.015 (1)	0.012 (1)	0.003 (1)	–0.001 (1)	–0.005 (1)
O12	0.011 (1)	0.015 (1)	0.013 (1)	–0.001 (1)	–0.000 (1)	–0.004 (1)
O13	0.016 (1)	0.017 (1)	0.014 (1)	–0.009 (1)	–0.001 (1)	–0.000 (1)
O14	0.016 (1)	0.017 (1)	0.014 (1)	0.008 (1)	0.001 (1)	0.001 (1)

Standard deviations are given in parentheses.

Table 4

Selected bond distances (Å) and bond angles (deg.) for YP_5O_{14}			
Tetrahedron around P1			
P1–O7	1.466 (3)	O7–P1–O8	122.1 (2)
P1–O8	1.483 (3)	O7–P1–O1	105.9 (1)
P1–O1	1.618 (3)	O8–P1–O1	108.3 (2)
P1–O2	1.638 (3)	O7–P1–O2	109.3 (2)
		O8–P1–O2	108.7 (2)
		O1–P1–O2	100.2 (1)
Tetrahedron around P2			
P2–O9	1.462 (3)	O9–P2–O4	114.9 (2)
P2–O4	1.560 (3)	O9–P2–O3	114.6 (2)
P2–O3	1.573 (3)	O4–P2–O3	103.7 (1)
P2–O2	1.574 (3)	O9–P2–O2	115.0 (2)
		O4–P2–O2	104.9 (1)
		O3–P2–O2	102.3 (2)
Tetrahedron around P3			
P3–O10	1.469 (3)	O10–P3–O11	122.6 (2)
P3–O11	1.481 (3)	O10–P3–O3	106.4 (2)
P3–O3	1.616 (3)	O11–P3–O3	109.6 (1)
P3–O5	1.640 (3)	O10–P3–O5	109.4 (2)
		O11–P3–O5	107.6 (2)
		O3–P3–O5	98.7 (14)
Tetrahedron around P4			
P4–O12	1.464 (3)	O12–P4–O6^{v}	115.6 (2)
P4–O6^{v}	1.557 (3)	O12–P4–O1^{vii}	113.0 (2)
P4–O1^{vii}	1.569 (3)	O6^{v}–P4–O1^{vii}	106.8 (1)
P4–O5	1.574 (3)	O12–P4–O5	116.6 (1)
		O6^{v}–P4–O5	101.5 (1)
		O1^{vii}–P4–O5	101.6 (1)
Tetrahedron around P5			
P5–O13	1.466 (3)	O13–P5–O14	121.8 (2)
P5–O14	1.471 (3)	O13–P5–O6	112.0 (2)
P5–O6	1.620 (3)	O14–P5–O6	104.4 (2)
P5–O4	1.631 (3)	O13–P5–O4	105.0 (1)
		O14–P5–O4	110.3 (2)
		O6–P5–O4	101.8 (1)

Selected bond distances (Å) and bond angles (deg.).			
Square antiprism around Y1		Dodecahedron around Y2	
Y1–O13^{i}	2.322 (3)	Y2–O14^{vi}	2.279 (3)
Y1–O13^{ii}	2.322 (3)	Y2–O14^{vii}	2.279 (3)
Y1–O7^{iii}	2.337 (3)	Y2–O11	2.356 (3)
Y1–O7^{iv}	2.337 (3)	Y2–O11^{v}	2.356 (3)
Y1–O9^{v}	2.353 (3)	Y2–O12	2.385 (3)
Y1–O9	2.353 (3)	Y2–O12^{v}	2.385 (3)
Y1–O8^{v}	2.363 (3)	Y2–O10^{viii}	2.393 (3)
Y1–O8	2.363 (3)	Y2–O10^{ix}	2.393 (3)
Intertetrahedral angles			
P4^{x}–O1–P1	131.0 (2)	P1–O8–Y1	147.4 (2)
P2–O2–P1	128.2 (2)	P2–O9–Y1	142.0 (2)
P2–O3–P3	133.9 (2)	P3–O10–Y2^{ix}	171.4 (2)
P2–O4–P5	137.5 (2)	P3–O11–Y2	138.4 (1)
P4–O5–P3	125.8 (2)	P4–O12–Y2	139.0 (2)
P4^{v}–O6–P5	141.2 (2)	P5–O13–Y1^{xi}	157.7 (2)
P4^{v}–O6–P5	141.2 (2)	P5–O13–Y1^{xi}	157.7 (2)
P1–O7–Y1^{iv}	148.1 (2)	P5–O14–Y2^{x}	150.0 (2)

Symmetry codes: (i) $x-1/2, y-1/2, z$; (ii) $-x+1/2, y-1/2, -z+1/2$; (iii) $x, -y+1, z+1/2$; (iv) $-x, -y+1, -z$; (v) $-x, y, -z+1/2$; (vi) $-x+1/2, y+1/2, -z+1/2$; (vii) $x-1/2, y+1/2, z$; (viii) $x, -y+2, z+1/2$; (ix) $-x, -y+2, -z$; (x) $x+1/2, y-1/2, z$; (xi) $x+1/2, y+1/2, z$.

It is worth noting that the shape of the 8-coordination polyhedra smoothly moves from the dodecahedron towards the square antiprism as the ionic radius of the trivalent ion decreases in this monoclinic $C2/c$ second family.

Although the LnP_5O_{14} ultraphosphates are divided into four structural types on the basis of their space groups, both I and III polymorphs are very close to each other, so the linking between the PO_4 tetrahedra and the LnO_8 polyhedra in their frameworks are identical. In both I and III polymorphs the LnO_8 polyhedra are isolated to each others as besides in all the LnP_5O_{14} ultraphosphates and are linked to PO_4 tetrahedra by corner-sharing. Each LnO_8 polyhedron is joined to four ribbons numbered from I to IV in Fig. 3a, first by sharing in the *bc*-plane two oxygens with two tetrahedra belonging to ribbon I, then by sharing in the *ac*-plane two other oxygens with two tetrahedra belonging to ribbons I and IV, respectively. This LnO_8 polyhedron is still connected to ribbons

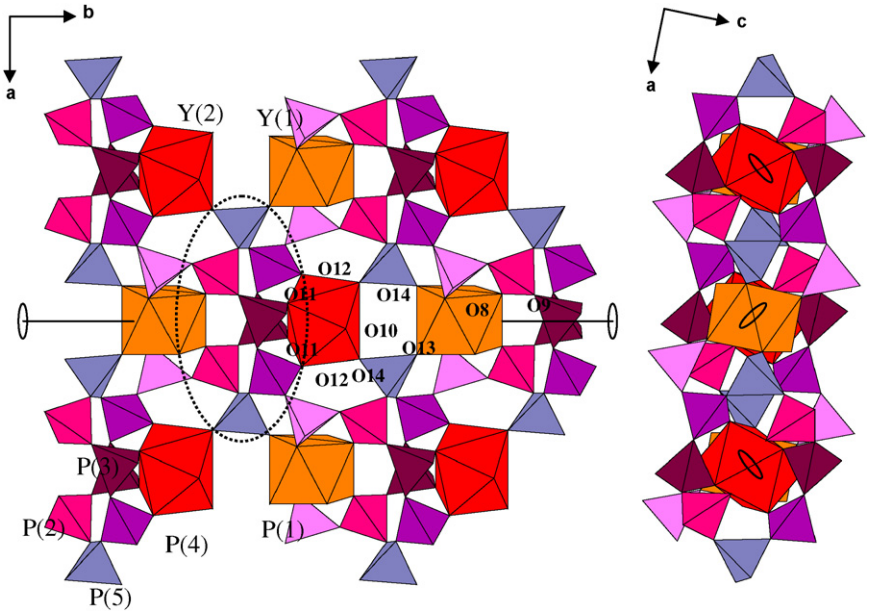

Fig. 1. Partial projection of the monoclinic ($C2/c$) structure of YP_5O_{14} showing the linking between the 8-membered PO_4 rings and the YO_8 polyhedra.

II and III by sharing two oxygens with two tetrahedra of each of these ribbons, on each side of the plane passing through the *Ln* rare earth and parallel to the *ac*-plane.

In the last IV structural type both LnO_8 types of coordination polyhedra are linked by corner-sharing to12-membered PO_4 rings in a very complex way as shown in Fig. 3b.

4.2. X-ray diffraction

Fig. 4 displays the X-ray powder pattern obtained from crystals as grown and roughly crushed. The whole pattern could have been indexed with the monoclinic $C2/c$ unit cell obtained from the crystal structure determination of the title compound. It is worth noting the strong intensities of the 0 0 l reflections.

However, this X-ray powder pattern is very different from that calculated from the atomic coordinates obtained by the refinement of the $C2/c$ monoclinic structure, nor matches the orthorhombic form (JCPDS card no. 25-1013). Fig. 5 shows the unexpected and surprising X-ray diffraction powder pattern obtained from the preceding sample by grinding it until it could pass through an 80 μm sieve. This powder pattern well matches with the calculated one for the $C2/c$ monoclinic YP_5O_{14} structure.

4.3. Thermal analysis

Both TGA (a) and DTA (b) thermographs are shown in Fig. 6. Gradual mass loss (~1%) is seen in the TGA thermal scan until approximately 760 °C due to steady release of adsorbed water and degassing. Afterwards a mass loss of 25% correlates with the significant endotherm centered at 926 °C and is realized as the result of the decomposition of the sample according to the scheme:

$$YP_5O_{14} \rightarrow Y(PO_3)_3 + P_2O_5$$

This is corroborated by the X-ray powder pattern recorded on the solid residue showing this one as being the yttrium polyphosphate $Y(PO_3)_3$ (JCPDF card no. 42-0501). This weight loss is also consistent with the theoretical value, i.e. 30.3%. This study confirms that the YP_5O_{14} ultraphosphate decomposes around 900 °C in perfect agreement with Durif [6] and Agrawal and Hummel [8] reports but is inconsistent with Fedorova et al. [7] results.

In some syntheses carried out at 450 °C and using a molar excess of 40% of ammonium dihydrogen phosphate, both the monoclinic ($C2/c$) and orthorhombic (*Pnma*) polymorphs could have simultaneously been obtained. Quenching of a dysphasic powdered sample heated at 700 °C in a sealed platinum tube results in the pure monoclinic phase. If the monoclinic polymorph is then annealed at 700 °C and slowly cooled to room temperature, the orthorhombic form reappears, showing the polymorphic transition orthorhombic ↔ monoclinic being reversible.

4.4. Spectroscopic analysis

Infrared and Raman spectra of YP_5O_{14} are shown in Figs. 7 and 8, respectively. Only the 1800–400 cm^{-1} range is relevant in both IR and Raman spectra. Noteworthy features of these two spectra are the presence of strong absorption bands in the 1280–1360, 920–1050, 620–800 and 400–590 cm^{-1} regions. They differ from those of other phosphates [27] in their distinctive absorption in the regions of stretching and deformation vibrations of the O–P–O and P–O–P bands. The bands of weak intensity near 1379 and 1324 cm^{-1}, respectively, on the IR and Raman spectra usually appear for ultraphosphates [28,29]. They are assigned to $\nu(P=O)$ vibrational mode. The observation of this vibrational mode is a good criterion to differentiate ultraphosphates from chain structure polyphosphates [30,31].

4.5. Optical properties

The emission spectrum of Eu^{3+} in $Y_{0.95}Eu_{0.05}P_5O_{14}$ (YP_5O_{14}:5% Eu^{3+}) was recorded at room temperature upon excitation in the $^5L_6$ level ($\lambda_{exc} = 395$ nm) in the spectral range 570–720 nm (Fig. 9). All observed lines are due to the transitions $^5D_0 \rightarrow {}^7F_J$ ($J = 0$–4) of the Eu^{3+} ion. An extension of this emission spectrum for the $^5D_0 \rightarrow {}^7F_1$ transition is shown as an inset in Fig. 9, for the $^5D_0 \rightarrow {}^7F_0$ and $^5D_0 \rightarrow {}^7F_1$ transitions. The number of $^5D_0 \rightarrow {}^7F_0$ and $^5D_0 \rightarrow {}^7F_1$ Stark components (two and six peaks are respectively observed) agrees with the presence of two crystallographic sites of C_2 symmetry, in which the Eu^{3+} ions are located.

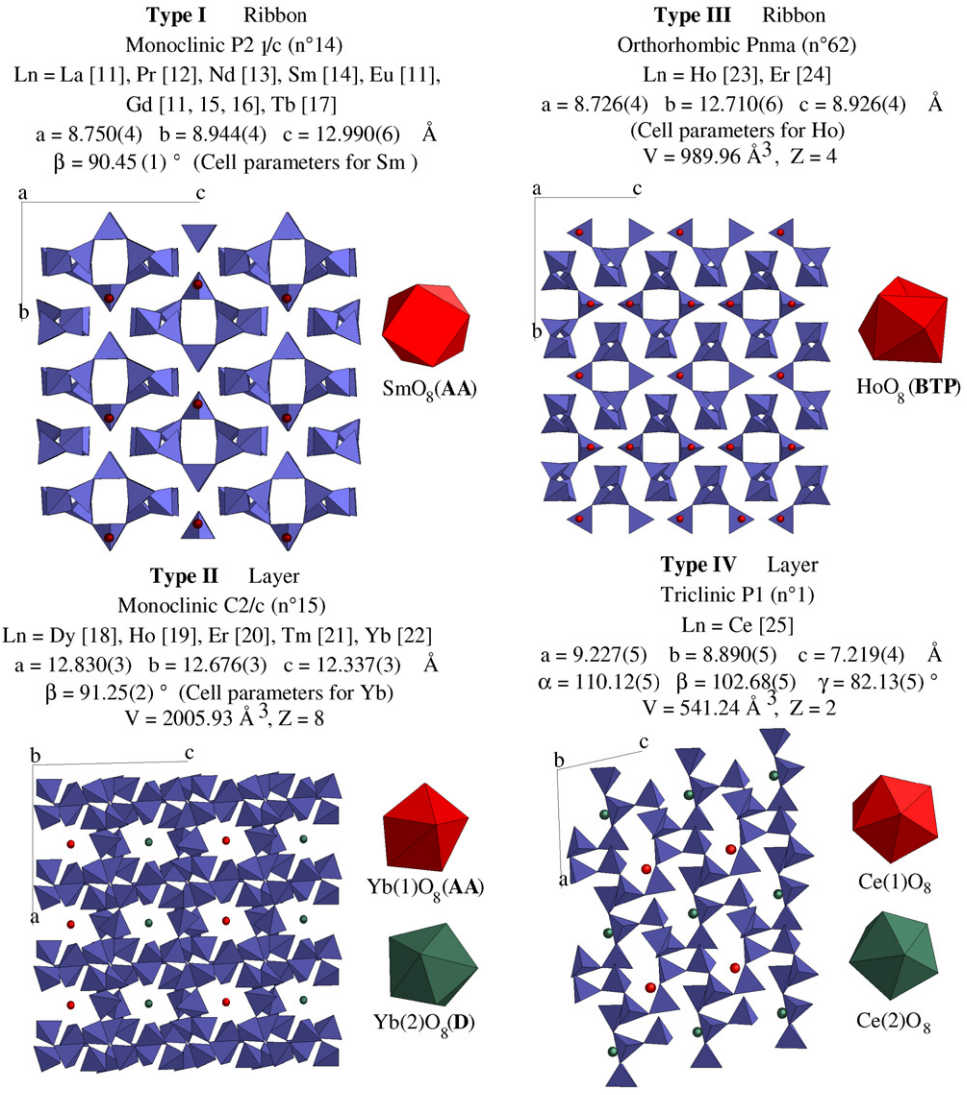

Fig. 2. Main crystallographic characteristics of the different structural types of the LnP_5O_{14} (Ln = rare earth, Y) ultraphosphates. D: dodecahedron; AA: Archimedean antiprism; BTP: bicapped trigonal prism [12,14–25].

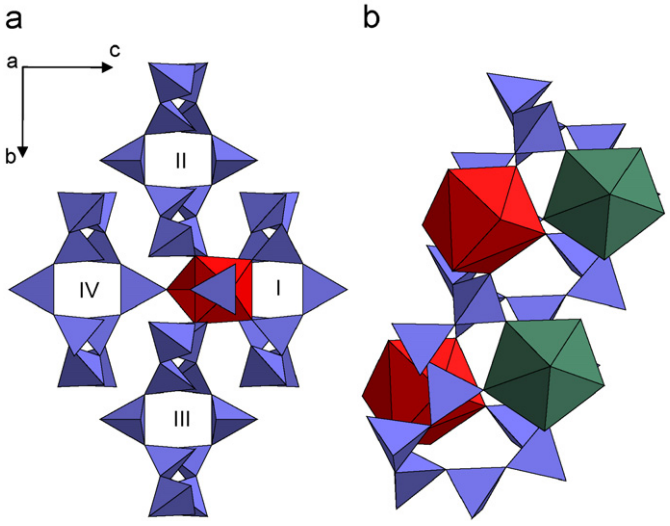

Fig. 3. Details of the linking between LnO_8 polyhedra and PO_4 groups in: (a) both monoclinic ($P2_1/c$) and orthorhombic (*Pnma*); (b) triclinic (P1) LnP_5O_{14} polymorphs.

Indeed, a C_2 point symmetry was evidenced for both Y^{3+} sites in the structural study of YP_5O_{14}. These preliminary optical results clearly show the agreement with the title structure description.

5. Conclusion

The crystal structure of the monoclinic *C*2/*c* polymorph of YP_5O_{14} has been refined from single-crystal data recorded on suitable crystal grown by reaction of Y_2O_3 with an excess of phosphoric acid. The subsequently calculated X-ray diffraction powder pattern has allowed to carry out a comprehensive study of the phase relationship in this ultraphosphate solid-state synthesis. The dimorphism of YP_5O_{14} is confirmed since crystals of both monoclinic (*C*2/*c*) and orthorhombic (*Pnma*) polymorphs could have been obtained by solid-state reaction using a molar excess of ammonium dihydrogen phosphate of at least 40%.

The luminescence properties of the Eu^{3+} ion used as local structural probe in monoclinic *C*2/*c* polymorph agree with the single-crystal structure determination. The results clearly indicate that the Eu^{3+} rare-earth ions are distributed over the two crystallographic sites of C_2 symmetry of the structure.

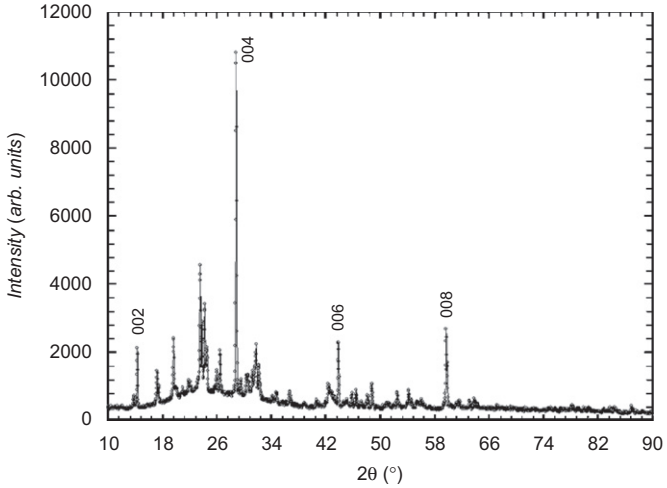

Fig. 4. X-ray diffraction powder pattern of YP_5O_{14}.

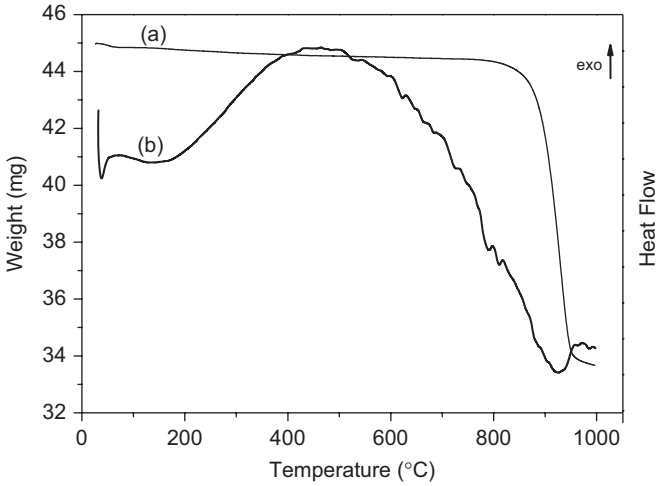

Fig. 6. TGA (a) and DTA (b) thermographs of YP_5O_{14}.

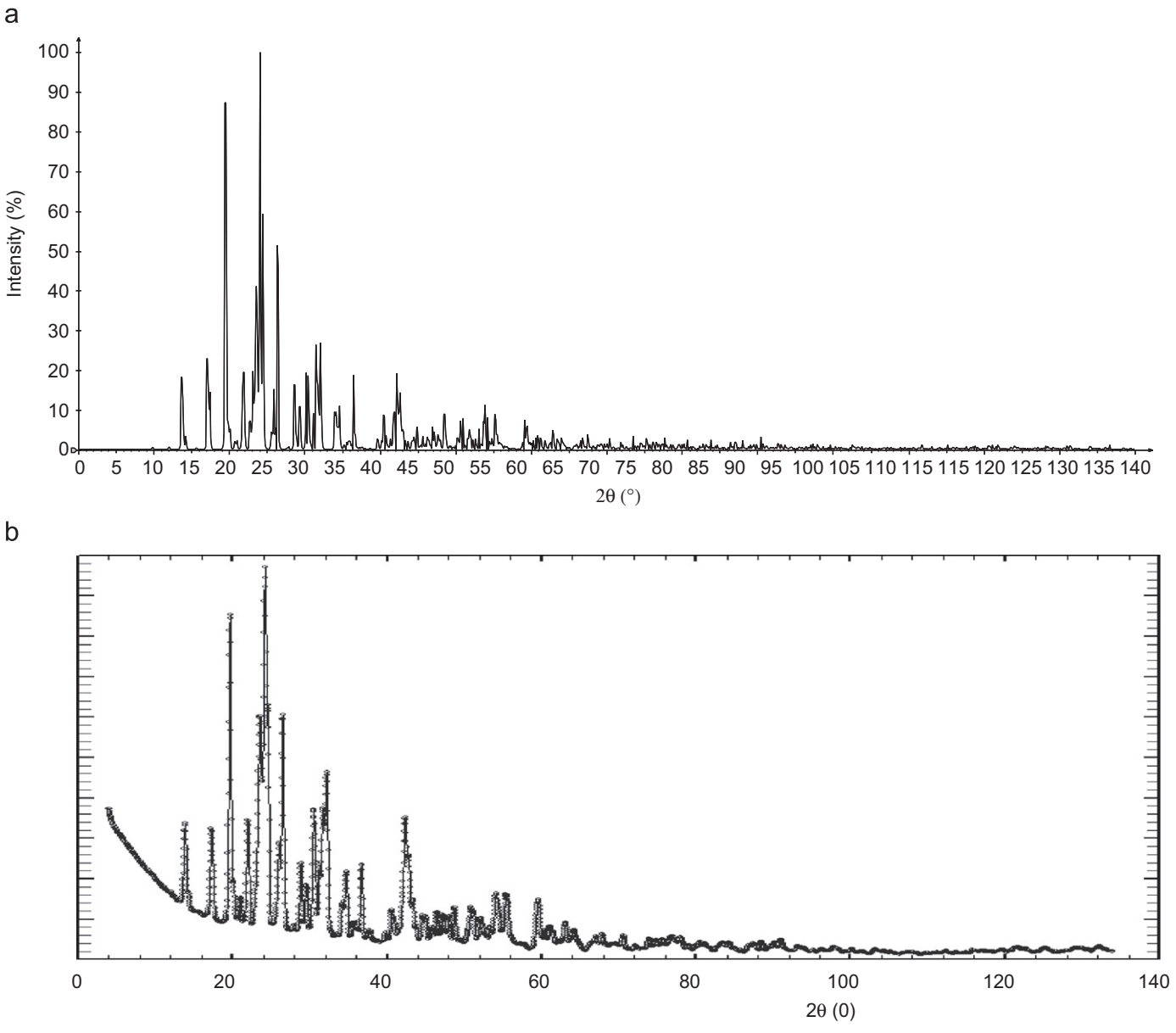

Fig. 5. Calculated (a) and experimental (b) X-ray diffraction powder patterns of monoclinic ($C2/c$) YP_5O_{14}.

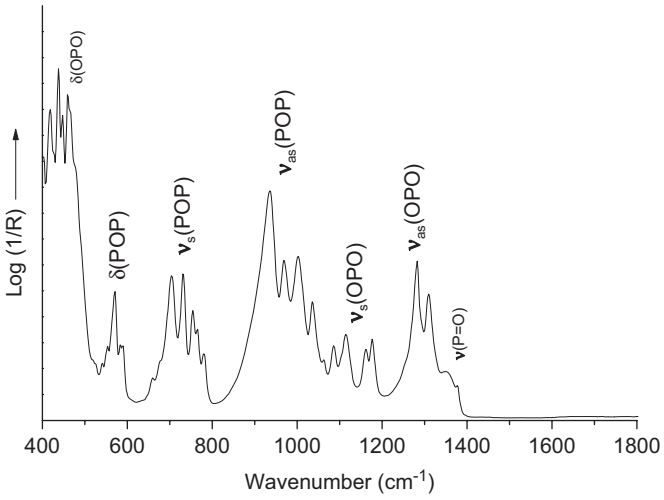

Fig. 7. IR spectrum of monoclinic ($C2/c$) YP_5O_{14} powder.

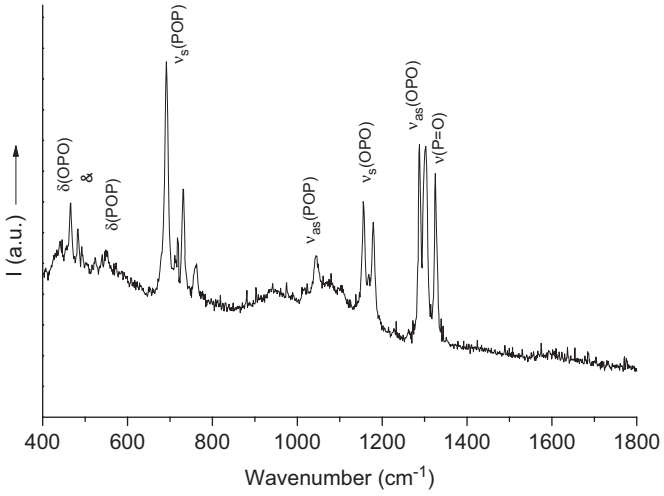

Fig. 8. Raman spectrum of monoclinic ($C2/c$) YP_5O_{14} powder.

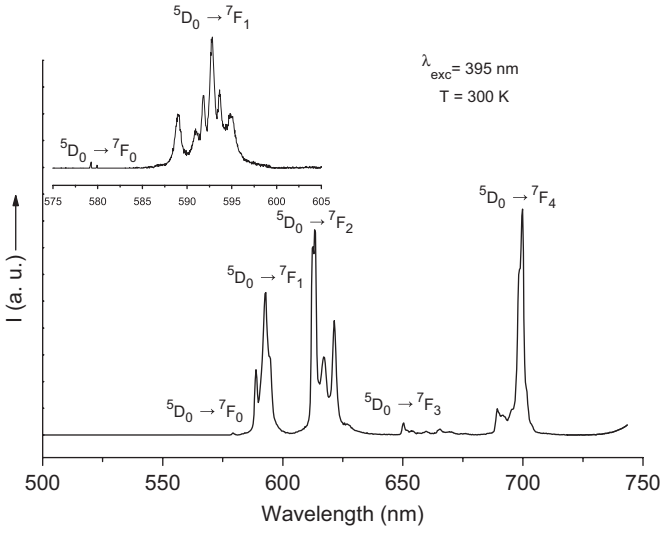

Fig. 9. Emission spectrum of YP_5O_{14}:5% Eu^{3+} at 300 K, under excitation into the $^5L_6$ level of Eu^{3+}. The inset shows an extension of this emission spectrum for the $^5D_0 \rightarrow {}^7F_1$ transition.

References

[1] H.P. Weber, T.C. Damen, H.G. Danielmeyer, B.C. Tofield, Appl. Phys. Lett. 22 (1973) 534.
[2] V.V. Ovsyankin, P.P. Feofilov, Sov. Phys. JETP Lett. 3 (1966) 322.
[3] F. Auzel, C. R. Acad. Sci. 262B (1966) 1016.
[4] M. Beucher, The rare earths elements, International Meeting, Paris, Grenoble, 1969.
[5] M. Bagieu-Beucher, D. Tranqui, Bull. Soc. Fr. Mineral. Cristallogr. 93 (1970) 505–508.
[6] A. Durif, Bull. Soc. Fr. Mineral. Cristallogr. 94 (1971) 314–318.
[7] E.N. Fedorova, L.K. Shmatok, I.I. Kozhina, T.R. Barabanova, Izv. Akad. Nauk. SSSR Neorg. Mater. 22 (1986) 480.
[8] D. Agrawal, F.A. Hummel, J. Electrochem. Soc. 127 (7) (1980) 1550.
[9] G.M. Sheldrick, SHELXS86. Program for the Solution of Crystal Structure, University of Göttingen, Germany, 1997.
[10] G.M. Sheldrick, SHELXL97, Program for the Refinement of Crystal Structures Using Single Crystal Diffraction Data, Göttingen University, Germany, 1997.
[11] J.M. Cole, M.R. Lees, J.A.K. Howard, R.J. Newport, G.A. Saunders, E. Schönherr, J. Solid State Chem. 150 (2000) 377–382.
[12] S. Liu, G. Hong, N. Hu, Acta Phys. Sin. 40 (1991) 64.
[13] H.Y.-P. Hong, Acta Crystallogr. B 30 (1974) 468–474.
[14] D. Tranqui, M. Bagieu, A. Durif, Acta Crystallogr. B 30 (1974) 1751–1755.
[15] H. Ettis, H. Naïli, T. Mhiri, Mater. Chem. Phys. 102 (2007) 275–280.
[16] Y. Lin, N. Hu, Q. Zhou, S. Wu, Chin. J. Appl. Chem. 1 (1983) 33.
[17] Y. Lin, N. Hu, M. Wang, E. Shi, Acta Chim. Sin. 40 (1982) 211.
[18] F. Chehimi-Moumen, M. Férid, Acta Crystallogr. E 63 (2007) i89–i91.
[19] M. Bagieu, I. Tordjman, A. Durif, G. Bassi, Cryst. Struct. Commun. 3 (1973) 387.
[20] B. Jezowska-Trzebiatowska, Z. Mazurak, T. Lis, Acta Crystallogr. B 36 (1980) 1639–1641.
[21] K.J. Zhou, Y.T. Qian, G.Y. Hong, Cryst. Struct. Commun. 11 (1982) 1695–1699.
[22] H.Y.-P. Hong, J.W. Pierce, Mater. Res. Bull. 9 (1974) 179–190.
[23] D. Tranqui, M. Bagieu Beucher, A. Durif, Bull. Soc. Fr. Mineral. Crystallogr. 95 (1972) 437.
[24] A. Katrusiak, F. Kaczmarek, Cryst. Res. Technol. 30 (1995) 501.
[25] M. Rzaigui, N. Kbir-Ariguib, M.T. Averbuch-Pouchot, A. Durif, J. Solid State Chem. 52 (1984) 61–65.
[26] M.A. Porai-Koshits, L.A. Aslanov, J. Struct. Chem. 13 (1972) 244–253.
[27] D.E.C. Corbridge, E.J. Lowe, J. Chem. Soc. (1954) 493.
[28] A. Sungur, M. Kizilyalli, D.S. Jones, J. Less-Common Met. 93 (1983) 441.
[29] F. Kaczmarek, M. Kaczmarski, J. Raman Spectrosc. 27 (1996) 645.
[30] R.K. Brow, D.R. Tallant, J.J. Hudgens, S.W. Martin, A.D. Irwin, J. Non-Cryst. Solids 177 (1994) 221.
[31] K. Meyer, J. Non-Cryst. Solids 209 (1997) 227.